Uniaxial pressure effect on the magnetic ordered moment and transition temperatures in BaFe_{2−x}T_{x}As_{2} (T=Co,Ni)

David W. Tam, Yu Song, Haoran Man, Sky C. Cheung, Zhiping Yin, Xingye Lu, Weiyi Wang, Benjamin A. Frandsen, Lian Liu, Zizhou Gong, Takashi U. Ito, Yipeng Cai, Murray N. Wilson, Shengli Guo, Keisuke Koshiishi, Wei Tian, Bassam Hitti, Alexandre Ivanov, Yang Zhao, Jeffrey W. Lynn, Graeme M. Luke, Tom Berlijn, Thomas A. Maier, Yasutomo J. Uemura, and Pengcheng Dai

Phys. Rev. B **95**, 060505 — Published 17 February 2017

DOI: 10.1103/PhysRevB.95.060505

Uniaxial pressure effect on the magnetic ordered moment and transition temperatures in $BaFe_{2-x}T_xAs_2$ (T =Co, Ni)

David W. Tam,[1,*] Yu Song,[1,*] Haoran Man,[1] Sky C. Cheung,[2] Zhiping Yin,[3] Xingye Lu,[1] Weiyi Wang,[1] Benjamin A. Frandsen,[2] Lian Liu,[2] Zizhou Gong,[2] Takashi U. Ito,[4] Yipeng Cai,[5] Murray N. Wilson,[5] Shengli Guo,[6] Keisuke Koshiishi,[7] Wei Tian,[8] Bassam Hitti,[9] Alexandre Ivanov,[10] Yang Zhao,[11,12] Jeffrey W. Lynn,[11] Graeme M. Luke,[5] Tom Berlijn,[13] Thomas A. Maier,[13] Yasutomo J. Uemura,[2] and Pengcheng Dai[1,3,†]

[1]*Department of Physics and Astronomy, Rice University, Houston, Texas 77005, USA*
[2]*Department of Physics, Columbia University, New York, New York 10027, USA*
[3]*Center for Advanced Quantum Studies and Department of Physics, Beijing Normal University, Beijing 100875, China*
[4]*Advanced Science Research Center, Japan Atomic Energy Agency, Tokai, Ibaraki 319-1195, Japan*
[5]*Department of Physics and Astronomy, McMaster University, Hamilton, Ontario L8S 4M1, Canada*
[6]*Department of Physics, Zhejiang University, Hangzhou 310027, China*
[7]*Department of Physics, Univeristy of Tokyo, 7-3-1 Hongo, Bunkyo-Ku, Tokyo 113, Japan*
[8]*Quantum Condensed Matter Division, Oak Ridge National Laboratory, Oak Ridge, Tennessee 37831, USA*
[9]*TRIUMF, Vancouver, British Columbia, V6T2A3, Canada*
[10]*Institut Laue-Langevin, 71 avenue des Martyrs, 38000 Grenoble, France*
[11]*NIST Center for Neutron Research, National Institute of Standards and Technology, Gaithersburg, Maryland 20899, USA*
[12]*Department of Materials Science and Engineering, University of Maryland, College Park, Maryland 20742, USA*
[13]*Center for Nanophase Materials Sciences and Computer Science and Mathematics Division, Oak Ridge National Laboratory, Oak Ridge, Tennessee 37831-6494, USA*

(Dated: January 4, 2017)

We use neutron diffraction and muon spin relaxation to study the effect of in-plane uniaxial pressure on the antiferromagnetic (AF) orthorhombic phase in $BaFe_2As_2$ and its Co- and Ni-substituted members near optimal superconductivity. In the low temperature AF ordered state, uniaxial pressure necessary to detwin the orthorhombic crystals also increases the magnetic ordered moment, reaching an 11% increase under 40 MPa for $BaFe_{1.9}Co_{0.1}As_2$, and a 15% increase for $BaFe_{1.915}Ni_{0.085}As_2$. We also observe an increase of the AF ordering temperature (T_N) of about 0.25 K/MPa in all compounds, consistent with density functional theory calculations that reveal better Fermi surface nesting for itinerant electrons under uniaxial pressure. The doping dependence of the magnetic ordered moment is captured by combining dynamical mean field theory with density functional theory, suggesting that the pressure-induced moment increase near optimal superconductivity is closely related to quantum fluctuations and the nearby electronic nematic phase.

PACS numbers: 74.70.Xa, 75.30.Gw, 78.70.Nx

Understanding the behavior of magnetism in iron superconductors continues to be an important topic in modern condensed matter physics because spin excitations may mediate electron pairing for high-temperature superconductivity [1–7]. Some of the earliest work in this field determined that iron pnictides such as LaFeAsO [1, 2] and $BaFe_2As_2$ [Figs. 1(a) and 1(b)] [3–5] form static stripe antiferromagnetic (AF) order at T_N preceded by a tetragonal-to-orthorhombic structural transition of the lattice at T_s ($T_N \leq T_s < 300$ K). While AF order may be a spin-density wave (SDW) from nesting of hole and electron Fermi surfaces at the Γ and X points in the one-iron Brillouin zone [Figs. 1(c) and 1(d)], respectively [8–11], it may also originate from localized moments on individual Fe sites [12–15].

Upon hole doping to form $Ba_{1-x}Na_xFe_2As_2$, a magnetically ordered state with restored tetragonal symmetry is found near optimal superconductivity, replacing the stripe AF ordered state [16, 17]. Mössbauer spectroscopy experiments find real space modulation of magnetic moments on Fe sites, thus conclusively establishing that the magnetic order with tetragonal symmetry is a SDW from itinerant electrons [18]. For electron doped $BaFe_{2-x}T_xAs_2$ (T =Co, Ni), long-range commensurate stripe magnetic order in $BaFe_2As_2$ evolves into short-range incommensurate magnetic order near optimal superconductivity [19, 20], due possibly to a SDW order [19] or a cluster spin glass [21–23]. While these results suggest a rich variety of magnetic ground states for superconducting iron pnicitdes, nematic order has recently been identified as a unifying feature near optimal superconductivity, seen via the resistivity anisotropy induced by in-plane mechanical strain [24]. Since nematic order couples linearly to anisotropic strain of the same symmetry [25, 26], a determination of the effect of uniaxial pressure on magnetism of iron pnictides should reveal if the observed nematic susceptibility [24] is associated with magnetic order and spin excitations.

Without uniaxial strain, $BaFe_{2-x}T_xAs_2$ forms twinned domains in the orthorhombic state, with AF Bragg re-

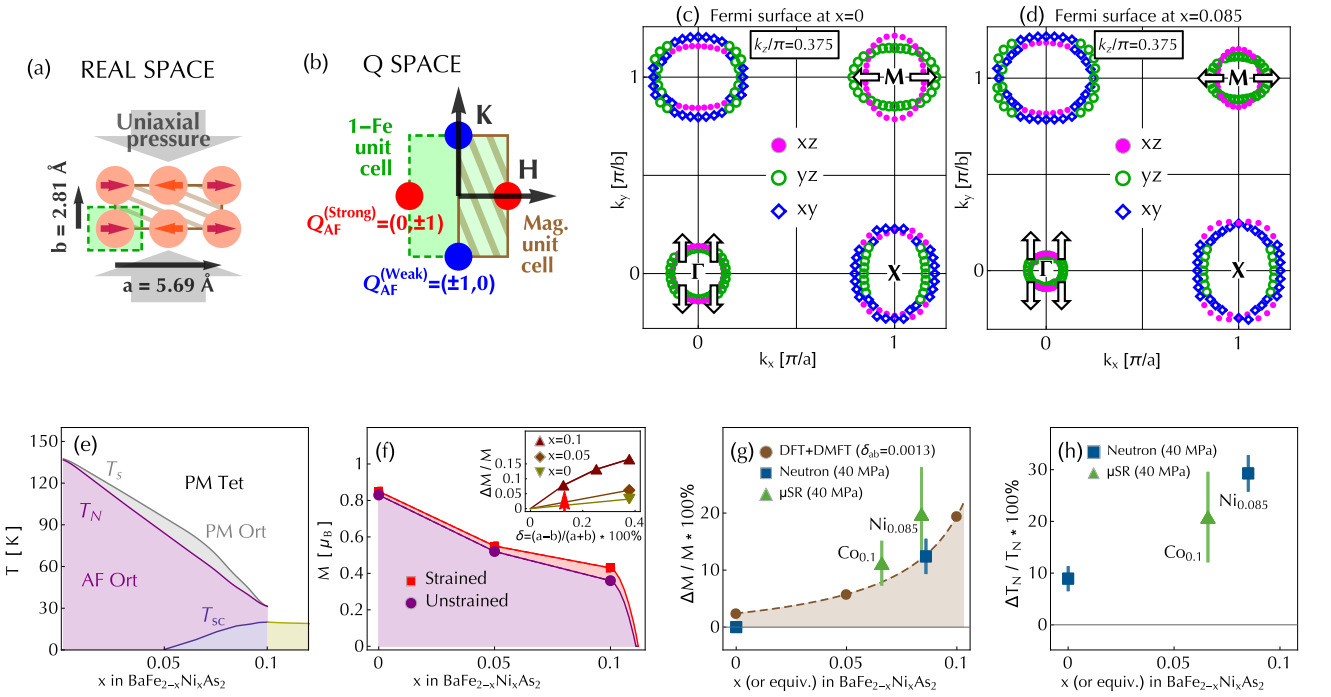

FIG. 1: (a-b) Real-space and **Q**-space configuration in the AF state, showing the majority domain Bragg reflections $\mathbf{Q}_{\rm strong} = (\pm 1, 0)$ in red dots for pressure applied along the b-axis, and the minority domain Bragg reflections $\mathbf{Q}_{\rm weak} = (0, \pm 1)$ as blue dots. (c-d) Schematic illustration of the uniaxial-pressure-induced Fermi surface distortion parallel to the ab-plane (at k_z=0.375π/c) for $BaFe_2As_2$ (c) and $BaFe_{1.915}Ni_{0.085}As_2$ (d). Arrows indicate the direction of distortion in this k_z plane for the uniaxially-strained case, which is much smaller than the thickness of the markers. Coloring shows the dominant orbital character as indicated in the inset. (e) Experimental phase diagram of $BaFe_{2-x}Ni_xAs_2$ [47]. (f) Electron-doping dependence of the ordered magnetic moment with (M; red) and without (M_0; purple) uniaxial pressure obtained from a combined DFT/DMFT calculation. The inset shows $\delta = (a-b)/(a+b)$ dependence of M/M_0 at $x = 0, 0.05$, and 0.1. (g) Theoretical/experimental results demonstrating the enhancement of $\Delta M/M$ as M decreases on approaching optimal doping [11]. (h) Enhancement of $\Delta T_N/T_N$, as T_N decreases on approaching optimal doping.

flections occurring at $(\pm 1, 0, L)$ and $(0, \pm 1, L)$ ($L = 1, 3, 5, \ldots$) [7]. Uniaxial pressure has been used to mechanically detwin single crystals by compressing along one axis of the orthorhombic lattice, creating a preferred orientation for microscopic domains [27–29]. However, even the modest amount of pressure necessary for detwinning (∼10 MPa) also induces a significant (∼1-2 K) upward shift of T_N in electron-doped $BaFe_2As_2$ [30–34], and changes T_s into a crossover with orthorhombic lattice distortion at all temperatures [35]. One study combining a phenomenological Ginsburg-Landau model with density functional theory (DFT) calculations under uniaxial strain suggest that the magnetic ordered moment of $BaFe_2As_2$ decreases under pressure [36], in agreement with the experimentally observed decrease in the combined magnetic scattering at $(\pm 1, 0, L)$ and $(0, \pm 1, L)$ [30, 31]. However, the bulk-averaged nature of neutron measurements cannot distinguish a change in magnetic volume fraction from a changing ordered moment. To conclusively determine the effect of uniaxial strain on magnetic order, one must combine neutron scattering with a probe such as muon spin relaxation (μSR) [37, 38].

In this paper, we use neutron diffraction, μSR, and combined DFT and dynamical mean field theory (DMFT) calculations [Figs. 1(f), 1(g), and 1(h)] [39, 40] to study the effect of uniaxial pressure on the AF phase transition in $BaFe_{2-x}T_xAs_2$. In $BaFe_2As_2$, the sample achieves nearly 100% detwinning for pressures above ∼10 MPa [Fig. 2(b)], while the ordered magnetic moment remains constant or reduces very slightly, resulting in a doubling of the neutron magnetic scattering intensity [Fig. 2(a)] from the majority-domain Bragg reflections $\mathbf{Q}_{\rm strong} = (\pm 1, 0)$ and elimination of magnetic scattering from the minority domains $\mathbf{Q}_{\rm weak} = (0, \pm 1)$ [Figs. 2(c) and 2(d)]. By contrast, in $BaFe_{1.915}Ni_{0.085}As_2$, the scattering intensity at $\mathbf{Q}_{\rm strong} = (\pm 1, 0)$ more than doubles for pressures greater than ∼30 MPa [Fig. 3(a)]. We also use μSR to show the magnetic volume fraction is not changing while the internal magnetic field at the muon site is increasing, conclusively establishing that the magnetic ordered moment is increasing under uniaxial strain. We also find the magnetic ordering temperature for dif-

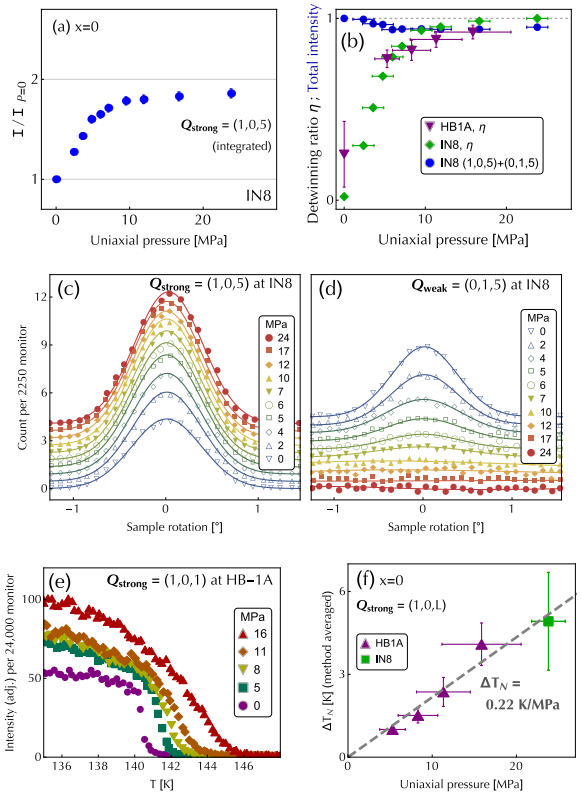

FIG. 2: (a) Intensity change of the $\mathbf{Q}_{\text{strong}} = (1, 0, 5)$ peak with uniaxial pressure on $BaFe_2As_2$ at IN8. (b) Detwinning ratio $\eta = (I_{\text{strong}} - I_{\text{weak}})/(I_{\text{strong}} + I_{\text{weak}})$ for both HB-1A and IN8 experiments, and the total intensity (circles) $I_{\text{strong}} + I_{\text{weak}}$ at IN8 which remains conserved, up to small corrections that we attribute to the extinction effect. (c-d) Rocking curves at $(1, 0, 5)$ and $(0, 1, 5)$ measured at IN8 at $T = 90$ K, demonstrating nearly 100% detwinning above 10 MPa. The solid lines are fits to a single Gaussian peak. (e) Temperature dependence of $\mathbf{Q}_{\text{strong}} = (1, 0, 1)$ on warming. For clarity, the vertical scale of each scan has been slightly adjusted to represent the total magnetic scattering intensity, using the integrated intensity of a rocking scan measured immediately prior to warming. (f) Shift in AF ordering temperature $\Delta T_N = T_N^{(\text{P})} - T_N^{(\text{P=0})}$ ($T_N^{(\text{P=0})} \approx 140$ K) for $BaFe_2As_2$ [11].

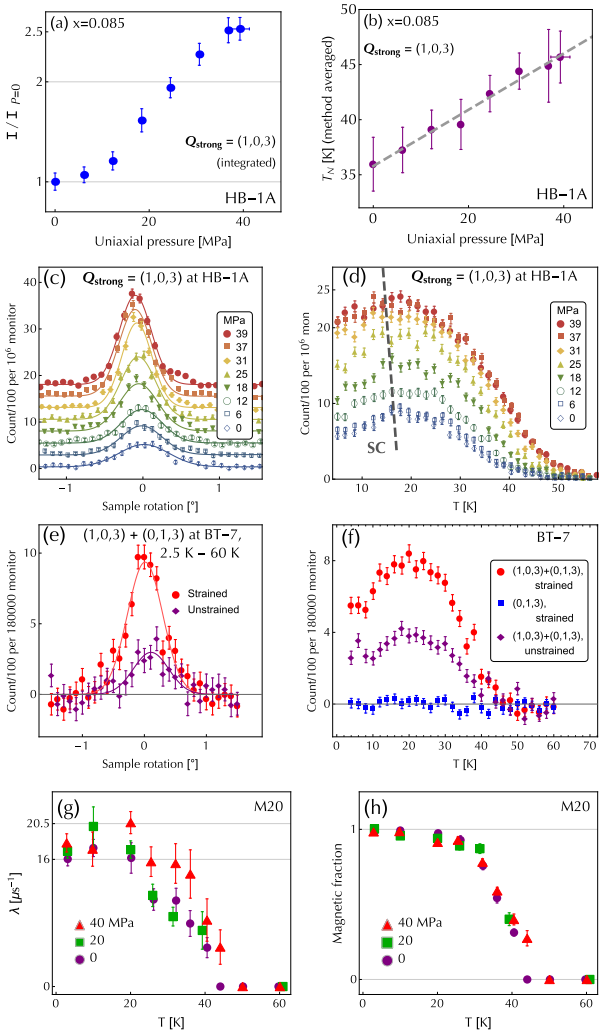

FIG. 3: (a) Intensity change of $\mathbf{Q}_{\text{strong}} = (1, 0, 3)$ with uniaxial pressure on $BaFe_{1.915}Ni_{0.085}As_2$ at HB-1A. (b) Shift in AF ordering temperature $\Delta T_N = T_N^{(\text{P})} - T_N^{(\text{P=0})}$ ($T_N^{(\text{P=0})} \approx 35$ K). (c) Rocking curves at $\mathbf{Q}_{\text{strong}} = (1, 0, 3)$, $T = 20$ K, measured at HB-1A in the $[H, 0, L]$ scattering plane. (d) Temperature scans at HB-1A. The dashed line in indicates the superconducting region ($T_c^{(40\text{ MPa})} - T_c^{(0)} \approx -3$ K) [11]. (e) Temperature dependence of the magnetic scattering intensity at $\mathbf{Q}_{\text{strong}} = (1, 0, 3)$ and $\mathbf{Q}_{\text{weak}} = (0, 1, 3)$ with and without pressure, measured in-situ at BT-7. (f) Combined rocking scans at $(1, 0, 3)$ and $(0, 1, 3)$. Data at 60 K has been subtracted from each $\mathbf{Q}$ position before combining the data. (g) Fast muon relaxation rate λ [11]. (h) Fast relaxing fraction V_M, demonstrating constant magnetic sample volume for all pressures below 35 K.

ferent iron pnictides [20] increases at approximately the same rate $T_N^{(\text{P})} - T_N^{(\text{P=0})} \approx 0.24$ K/MPa [Fig. 2(f) and 3(b)], consistent with our DFT calculations of the nesting condition under pressure [11]. Our μSR measurements also demonstrate that the AF phase transition is broadened, indicating that the internal uniaxial strain has a distribution for a nominally constant induced stress.

For our combined DFT and DMFT calculations in the collinear AF state, we use the experimental crystal structure and the same Coulomb interactions used previously for $BaFe_2As_2$ [39, 40]. We find that uniaxial strain does indeed enhance the ordered moment for $BaFe_{1.915}Ni_{0.085}As_2$ (Fig. 3), and that the effect becomes larger for samples close to optimal superconductivity. The inset in Figure 1(f) shows the dependence of the ordered magnetic moment on doping (x) and distortion ($\delta = (a - b)/(a + b)$), which supports a much larger increase of the magnetic moment in the doped compounds for fixed $\delta = 0.38\%$, corresponding to about 30 MPa in the parent compound. In Figure 1(f), we fix the dis-

tortion $\delta = 0.0013$ corresponding to about 10 MPa in the parent compound [35], and plot the ordered moment with (M at $a > b$) and without uniaxial pressure (M_0 at $a = b$). Using these results, in Fig. 1(g) we define a susceptibility $\chi = [(M - M_0)/(M + M_0)]/[(a - b)/(a + b)]$, which is small in the parent compound but shows diverging behavior near $x = 0.1$ (dashed line). Because fixing the distortion $\delta = 0.0013$ corresponds to a greater applied uniaxial pressure for the doped samples due to the larger bulk modulus in those compounds [26], the overplotted experimental points from neutron and μSR measurements may underestimate the moment increase relative to the calculated points. Nevertheless, we find clear similarity between the theoretical and experimental results, implying that the divergence of the nematic susceptibility [24] have a magnetic origin.

Figure 1(e) shows the schematic phase diagram of $BaFe_{2-x}Ni_xAs_2$, where Fig. 1(a) and 1(b) show the AF unit cell and Bragg peak positions in reciprocal space, respectively [7]. By gradually applying uniaxial pressure along the b-axis direction of the orthorhombic structure, the sample becomes increasingly detwinned, which enhances the $\mathbf{Q}_{\rm strong} = (\pm 1, 0)$ Bragg peak while the $\mathbf{Q}_{\rm weak} = (0, \pm 1)$ peaks become extinguished [red and blue dots in Fig. 1(b)] [30–33]. The striped brown boxes in Fig. 1(a-b) represent the low-temperature magnetic unit cell and its equivalent area in $\mathbf{Q}$ space, while in green we show the configurations for a single Fe ion [11].

Figure 2 summarizes our experimental results on the uniaxial pressure effect in $BaFe_2As_2$. In Fig. 2(c) and 2(d), we show how the Bragg peak intensity becomes redistributed from the weak side [$\mathbf{Q}_{\rm weak} = (0, \pm 1, L)$] to the strong side [$\mathbf{Q}_{\rm strong} = (\pm 1, 0, L)$], resulting in a near doubling of the strong reflection intensity [Fig. 2(a)] while the total intensity remains conserved [Fig. 2(b)]. Consistent with earlier work [30, 31], we find that pressure both enhances and broadens the magnetic phase transition. The rocking curves [Fig. 2(c-d)] at $(1, 0, 5)$ and $(0, 1, 5)$ were collected at IN8 at 90 K [34]. The pressure dependence of the detwinning ratio, defined as $\eta = (I_{10} - I_{01})/(I_{10} + I_{01})$, and total scattering intensity $I_{\rm total} = (I_{10} + I_{01})/(I_{10} + I_{01})_{P=0}$ from both experiments are also included in Fig. 2(b), which shows a very small reduction in $I_{\rm total}$ between 0 and 5 MPa. Fig. 2(e-f) shows the effect of pressure on the magnetic ordering temperature [11].

Figure 3 summarizes the uniaxial pressure dependence in $BaFe_{1.915}Ni_{0.085}As_2$. In a twinned sample, the elastic magnetic scattering intensity at $(1, 0, 3)$ should be equal to that at $(0, 1, 3)$, ignoring absorption and other instrumentation effects [11]. If magnetic moments do not react to the applied uniaxial pressure, one would expect the scattering intensity for a fully detwinned sample to at most double at the $(1, 0, 3)$ position, such as in Fig. 2(a) for $BaFe_2As_2$. Figure 3(a) shows this is not the case: the scattering intensity at 20 K rises by a factor of $\sim$2.5 from 0 to 40 MPa. Considering the detwinning effect, this corresponds to a 25% increase in the scattering cross-section, which is proportional to the squared magnetic ordered moment (M^2). Fig. 3(c-d) shows the temperature dependence of the strong Bragg reflection, measured in the $[H, 0, 0] \times [0, 0, L]$ scattering plane, which decreases below 20 K due to the onset of superconductivity [41, 42]. There is also a slight decrease in T_c under uniaxial pressure [11, 43]. Figure 3(e-f) shows that the combined scattering from $\mathbf{Q}_{\rm strong}$ and $\mathbf{Q}_{\rm weak}$ nearly doubles in intensity from zero to large uniaxial pressure (> 50 MPa) [11]. Using these data and the measured magnetic moment of $M = 0.08\ \mu_B$/Fe for $BaFe_{1.915}Ni_{0.085}As_2$ [20], we estimate an increase in magnetic moment from 0.08 μ_B/Fe to 0.092 μ_B/Fe.

To disentangle the magnetic volume fraction from the ordered moment in $BaFe_{1.915}Ni_{0.085}As_2$, we carried out μSR measurements using the same crystal and under the same conditions [11]. We implanted muons with the spin polarization along the sample a-axis and observed fast relaxation due to a build-up of the static internal magnetic field. From the ZF-μSR time spectra in [11], we obtained the fast relaxation rate λ in Fig. 3(g), which is linearly proportional to the size of the local static magnetic moment (M), together with the volume fraction V_M of magnetically ordered regions in Fig. 3(h). In addition to confirming the pressure-induced T_N increase [Fig. 1(h)], we find that the relaxation rates at $T = 20$ K and $T = 3$ K exhibit a $\sim$10-20% increase from 2.5 MPa to 40 MPa [11], and see a decreasing trend in λ below T_c. These μSR results are consistent with the neutron results, where the $\sim$25% increase from 2.5 MPa to 40 MPa (after detwinning is considered) is seen in the scattering intensity [Fig. 3(a)], proportional to M^2. The fraction of the sample exhibiting magnetic order [Fig. 3(h)] is essentially 100% below $T = 35$ K with no dependence on uniaxial pressure, while it is slightly larger and broader in the region $30 < T < 50$ K under pressure, consistent with the results of neutron scattering [Fig. 2(e), 3(d), 3(f), and 3(g)] [30, 31].

We carried out similar μSR measurements on $BaFe_{1.9}Co_{0.1}As_2$ ($T_N = 70$ K). In a zero field environment, we observe oscillations in the time spectra that indicate the presence of long-range order, different from the spectra in $BaFe_{1.915}Ni_{0.085}As_2$ [11] where the larger doping causes the magnetic fields to lose coherence [35, 37, 38, 45, 46]. Assuming two muon stopping sites in $BaFe_{2-x}Co_xAs_2$ [45], we fit the short-time coherent relaxation with a two-cosine function, separately fitting both frequencies for each temperature and uniaxial pressure, while globally constraining the other free parameters such as relaxation rates [11]. Figure 4(a) shows the uniaxial pressure evolution of the fast cosine frequency in the muon decay time-spectra [Fig. 4(b)] for several temperatures. Although 2 K is below T_c, the magnetic field increases at least as much as at 25 K, indicating that

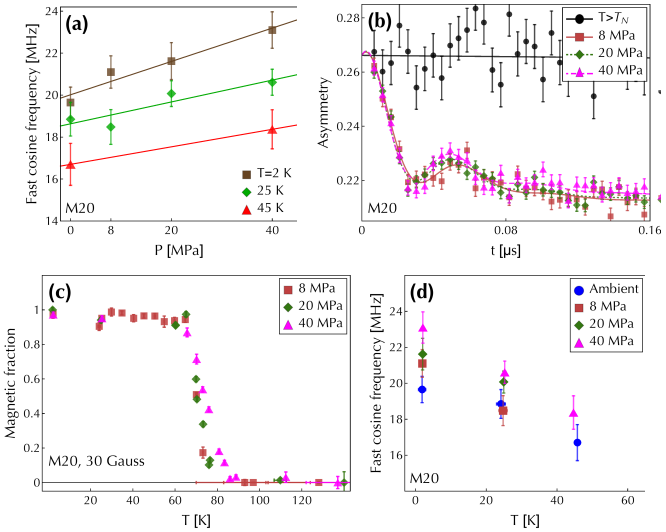

FIG. 4: (a) Increase of the oscillation frequency in the fast-relaxing portion of the muon decay asymmetry, for $T = 2$ K (superconducting), 25 K, and 45 K for $BaFe_{1.9}Co_{0.1}As_2$ [11]. (b) Muon decay asymmetry at 25 K as a function of uniaxial pressure. The fraction of muons remaining polarized in this short time window are those landing in the nonmagnetic sample holder. (c) Fast relaxing fraction of muons in a 30 G transverse magnetic field, demonstrating a constant magnetic sample volume below T_N=65 K, as well as a broadening of the magnetic transition under pressure and an increase in T_N. (d) Data in (a) plotted as an order parameter.

the magnetic phase may not be fully saturated at 25 K. To measure the magnetic volume fraction [Fig. 4(c)], we apply a weak (30 G) external magnetic field in order to clearly distinguish the fast relaxing component from the long paramagnetic oscillations. The ordered phase volume saturates below $\sim$ 65 K for all pressures, while for higher temperatures the magnetic transition is broadened significantly for $BaFe_{1.9}Co_{0.1}As_2$ as it was with $BaFe_{1.915}Ni_{0.085}As_2$ [Fig. 3(h)].

As the doping increases and the ordered magnetic moment correspondingly decreases, it is natural to expect that quantum fluctuations, including those related to a nematic quantum critical point [24], become important. Here we have demonstrated that an in-plane symmetry-breaking field is more effective in enhancing the ordered magnetic moment for nearly optimally doped iron pnictides. The corresponding decrease in T_c is consistent with the view that by slightly increasing the orthorhombicity, the doped system effectively shifts leftward on the phase diagram (toward the parent compound), and demonstrates that in-plane lattice distortion is a mechanism by which magnetism directly competes with superconductivity. Since the doped compounds react much more sensitively to uniaxial pressure, the enhanced magnetic properties demonstrate the sensitivity of magnetism to quantum fluctuations near optimal superconductivity, suggesting that nematic order is associated with both magnetism and optimal superconductivity in iron pnictides [24, 25].

The neutron scattering work at Rice is supported by the U.S. NSF-DMR-1362219 and DMR-1436006 (P.D.). The RPA calculations at Rice/ORNL is supported by NSF-DMR-1308603 (T.A.M. and P.D.). The materials synthesis efforts at Rice is supported by the Robert A. Welch Foundation Grant Nos. C-1839 (P.D.). The research at ORNL was sponsored by the Scientific User Facilities Division, Office of BES, U.S. DOE. The DFT and Wannier function calculations were conducted at the Center for Nanophase Materials Sciences, which is a DOE's Scientific User Facility (T.B.). Work at Columbia and TRIUMF is supported by NSF-DMREF DMR-1436095 and DMR-1610633 (Y.J.U.), JAEA Reimei project and Friends of U. Tokyo Inc.

* These authors contributed equally to this work
† Electronic address: pdai@rice.edu

[1] Y. Kamihara, T. Watanabe, M. Hirano, and H. Hosono, J. Am. Chem. Soc. **130**, 3296-3297 (2008).
[2] C. de la Cruz *et al.*, Nature (London) **453**,899 (2008).
[3] Q. Huang, Y. Qiu, W. Bao, M. A. Green, J. W. Lynn, Y. C. Gasparovic, T. Wu, G. Wu, and X. H. Chen, Phys. Rev. Lett. **101**, 257003 (2008).
[4] S. D. Wilson, Z. Yamani, C.R. Rotundu, B. Freelon, E. Bourret-Courchesne, and R.J. Birgeneau, Phys. Rev. B **79**, 184519 (2009).
[5] M. G. Kim, R. M. Fernandes, A. Kreyssig, J. W. Kim, A. Thaler, S. L. Bud'ko, P. C. Canfield, R. J. McQueeney, J. Schmalian, and A. I. Goldman, Phys. Rev. B **83**, 134522 (2011).
[6] D. J. Scalapino, Rev. Mod. Phys. **84**, 1383 (2012).
[7] P. C. Dai, Rev. Mod. Phys. **87**, 855 (2015).
[8] I. I. Mazin, M. D. Johannes, L. Boeri, K. Koepernik, and D. J. Singh, Phys. Rev. B **78**, 085104 (2008).
[9] P. J. Hirschfeld, M. M. Korshunov, I. I. Mazin, Rep. Prog. Phys. **74**, 124508 (2011).
[10] A. Chubukov, Ann. Rev. Condens. Matter Phys. **3**, 57 (2012).
[11] For additional data and analysis, see supplementary information.
[12] Q. Si and E. Abrahams, Phys. Rev. Lett. **101**, 076401 (2008).
[13] C. Fang, H. Yao, W. F. Tsai, J. P. Hu, and S. A. Kivelson, Phys. Rev. B **77**, 224509 (2008).
[14] C. K. Xu, M. Müller, and S. Sachdev, Phys. Rev. B **78**, 020501(R) (2008).
[15] D. N. Basov and A. V. Chubukov, Nat. Phys. **7**, 272 (2011).
[16] S. Avci, O. Chmaissem, J. M. Allred, S. Rosenkranz, I. Eremin, A. V. Chubukov, D. E. Bugaris, D. Y. Chung, M.G. Kanatzidis, J.-P Castellan, J. A. Schlueter, H. Claus, D. D. Khalyavin, P. Manuel, A. Daoud-Aladine, and R. Osborn, Nat. Comm. **5**, 3845 (2013).
[17] F. Waβer, A. Schneidewind, Y. Sidis, S. Wurmehl, S. Aswartham, B. Buchner, and M. Braden, Phys. Rev. B **91**, 060505(R) (2015).

[18] J. M. Allred, K. M. Taddei, D. E. Bugaris, M. J. Krogstad, S. H. Lapidus, D. Y. Chung, H. Claus, M. G. Kanatzidis, D. E. Brown, J. Kang, R. M. Fernandes, I. Eremin, S. Rosenkranz, O. Chmaissem, and R. Osborn, Nature Physics **12**, 493 (2016).

[19] D. K. Pratt, M. G. Kim, A. Kreyssig, Y. B. Lee, G. S. Tucker, A. Thaler, W. Tian, J. L. Zarestky, S. L. Bud'ko, P. C. Canfield, B. N. Harmon, A. I. Goldman, and R. J. McQueeney, Phys. Rev. Lett. **106**, 257001 (2012).

[20] H. Q. Luo, R. Zhang, M. Laver, Z. Yamani, M. Wang, X. Y. Lu, M. Y. Wang, Y. Chen, S. L. Li, S. Chang, J. W. Lynn, and P. C. Dai, Phys. Rev. Lett. **108**, 247002 (2012).

[21] A. P. Dioguardi, J. Crocker, A. C. Shockley, C. H. Lin, K. R. Shirer, D. M. Nisson, M. M. Lawson, N. apRoberts-Warren, P. C. Canfield, S. L. Bud'ko, S. Ran, and N. J. Curro, Phys. Rev. Lett. **111**, 207201 (2013).

[22] A. P. Dioguardi, M. M. Lawson, B. T. Bush, J. Crocker, K. R. Shirer, D. M. Nisson, T. Kissikov, S. Ran, S. L. Bud'ko, P. C. Canfield, S. Yuan, P. L. Kuhns, A. P. Reyes, H.-J. Grafe, and N. J. Curro, Phys. Rev. B **92**, 165116 (2015).

[23] X. Y. Lu, D. W. Tam, Chenglin Zhang, Huiqian Luo, Meng Wang, Rui Zhang, Leland W. Harriger, T. Keller, B. Keimer, L.-P. Regnault, Thomas A. Maier, and P. C. Dai, Phys. Rev. B **90**, 024509 (2014).

[24] H.-H. Kuo, J.-H. Chu, J.C. Palmstrom, S.A. Kivelson, and I.R. Fisher, Science **352**, 958 (2016).

[25] R. M. Fernandes, A. V. Chubukov, and J. Schmalian, Nat. Phys. **10**, 97 (2014).

[26] A. E. Böhmer and C. Meingast, Comptes Rendus Physique **17**, 90 (2016).

[27] J. H. Chu *et al.*, Science **329**, 824 (2010).

[28] M. A. Tanatar, E. C. Blomberg, A. Kreyssig, M. G. Kim, N. Ni, A. Thaler, S. L. Bud'ko, P. C. Canfield, A. I. Goldman, I. I. Mazin, and R. Prozorov, Phys. Rev. B **81**, 184508 (2010).

[29] I. R. Fisher, L. Degiorgi, and Z. X. Shen, Rep. Prog. Phys. **74**, 124506 (2011).

[30] C. Dhital, Z. Yamani, W. Tian, J. Zeretsky, A. S. Sefat, Z. Wang, R. J. Birgeneau, and S. D. Wilson, Phys. Rev. Lett. **108**, 087001 (2012).

[31] C. Dhital, T. Hogan, Z. Yamani, R. J. Birgeneau, W. Tian, M. Matsuda, A. S. Sefat, Z. Wang, and S. D. Wilson, Phys. Rev. B **89**, 214404 (2014).

[32] Y. Song, S. V. Carr, X. Y. Lu, C. L. Zhang, Z. C. Sims, N. F. Luttrell, S. X. Chi, Y. Zhao, J. W. Lynn, and P. C. Dai, Phys. Rev. B **87**, 184511 (2013).

[33] X. Y. Lu, J. T. Park, R. Zhang, H. Q. Luo, A. H. Nevidomskyy, Q. Si, and P. C. Dai, Science **345**, 657 (2014).

[34] H. R. Man, X. Y. Lu, J. S. Chen, R. Zhang, W. L. Zhang, H. Q. Luo, J. Kulda, A. Ivanov, T. Keller, E. Morosan, Q. Si, and P. C. Dai, Phys. Rev. B **92**, 134521 (2015).

[35] X. Y. Lu, K. F. Tseng, T. Keller, W. L. Zhang, D. Hu, Y. Song, H. R. Man, J. T. Park, H. Q. Luo, S. L. Li, A. N. Nevidomskyy, and P. C. Dai, Phys. Rev. B **93**, 134519 (2016).

[36] M. Tomic, H. O. Jeschke, R. M. Fernandes, and R. Valenti, Phys. Rev. B **87**, 174503 (2013).

[37] T. Goko, A.A. Aczel, E. Baggio-Saitovitch, S.L. Bud'ko, P.C. Canfield, J.P. Carlo, G.F. Chen, P. Dai, A.C. Hamann, W.Z. Hu, H. Kageyama, G.M. Luke, J.L. Luo, B. Nachumi, N. Ni, D. Reznik, D.R. Sanchez-Candela, A.T. Savici, K.J. Sikes, N.L. Wang, C.R. Wiebe, T.J. Williams, T. Yamamoto, W. Yu, and Y.J. Uemura, Phys. Rev. B **80**, 024508 (2009).

[38] A.A. Aczel, E. Baggio-Saitovitch, S.L. Budko, P.C. Canfield, J.P. Carlo, G.F. Chen, P. Dai, T. Goko, W.Z. Hu, G.M. Luke, J.L. Luo, N. Ni, D.R. Sanchez-Candela, F.F. Tafti, N.L. Wang, T.J. Williams, W. Yu, and Y.J. Uemura, Phys. Rev. B **78**, 214503 (2008).

[39] Z. P. Yin, K. Haule, and G. Kotliar, Nat. Mater. **10**, 932 (2011).

[40] Z. P. Yin, K. Haule, G. Kotliar, Nat. Phys. **10**, 845 (2014).

[41] D. K. Pratt, W. Tian, A. Kreyssig, J. L. Zarestky, S. Nandi, N. Ni, S. L. Bud'ko, P. C. Canfield, A. I. Goldman, and R. J. McQueeney, Phys. Rev. Lett. **103**, 087001 (2009).

[42] A. D. Christianson, M. D. Lumsden, S. E. Nagler, G. J. MacDougall, M. A. McGuire, A. S. Sefat, R. Jin, B. C. Sales, and D. Mandrus, Phys. Rev. Lett. **103**, 087002 (2009).

[43] F. Hardy, P. Adelmann, Th. Wolf, H. v. Löhneysen, and C. Meingast, Phys. Rev. Lett. **102**, 187004 (2009).

[44] H.-H. Kuo and I.R. Fisher, Phys. Rev. Lett. **112**, 227001 (2014).

[45] T.J. Williams, A.A. Aczel, S.L. Bud'ko, P.C. Canfield, J.P. Carlo, T. Goko, Y.J. Uemura, and G.M. Luke, arXiv:1408.3643 [cond-Mat] (2014).

[46] T.J. Williams, A.A. Aczel, E. Baggio-Saitovitch, S.L. Bud'ko, P.C. Canfield, J.P. Carlo, T. Goko, J. Munevar, N. Ni, Y.J. Uemura, W. Yu, and G.M. Luke, Phys. Rev. B **80**, 094501 (2009).

[47] X. Lu, H. Gretarsson, R. Zhang, X. Liu, H. Luo, W. Tian, M. Laver, Z. Yamani, Y.-J. Kim, A.H. Nevidomskyy, Q. Si, and P. Dai, Phys. Rev. Lett. **110**, 257001 (2013).